Experiments in Fluids 32 (2002) 652–666 © Springer-Verlag 2002
DOI 10.1007/s00348-002-0405-z

Ultra-fast-framing schlieren system for studies of the time evolution of jets in supersonic crossflows

A. Ben-Yakar, R.K. Hanson

Abstract A new ultra-fast camera system is used to study the time evolution of jets in supersonic crossflows via schlieren imaging. The commercial high-speed camera includes eight independent intensified charged couple devices (ICCDs) and is capable of acquiring images at rates up to 100 MHz. A long-duration (up to 200 μs) xenon flashlamp is used as the continuous light source. The exposure times of the ICCDs and the interframing times were designed to achieve schlieren images with high spatial and temporal resolution. Example data are presented for a hydrogen jet injected into a high total enthalpy supersonic crossflow, generated using a short-duration impulse facility (expansion tube). The large-eddy convection characteristics of the jet, its penetration and the unsteady nature of the shock wave around it are analyzed. Temporal correlations, such as the movement of organized (coherent) structures and fluctuations in the bow-shock, are readily perceived by assembling the eight consecutive images as a movie (http://navier.stanford.edu/hanson/propulsion/scramjet/movies/t1179.html).

List of symbols

a, b	eddy dimensions
d	jet orifice diameter
F	Fourier transform of image 2
G	Fourier transform of image 1
G^*	conjugate G
J	jet to free-stream momentum flux ratio, $=(\gamma pM^2)_j/(\gamma pM^2)_\infty$
M	Mach number
p	static pressure
R	cross-correlation of image 1 and image 2
Re_d	jet Reynolds number at the injection exit, $=(\rho_j U_j d)/\mu_j$
Re_x	free-stream Reynolds number at the injection location, $=(\rho_\infty U_\infty x)/\mu_\infty$
T	static temperature
U	velocity
U_c	convection velocity
γ	specific heat ratio
δ	boundary layer thickness
λ	eddy wavelength
μ	dynamic viscosity
θ	eddy orientation angle
ρ	density
Δx, Δy	cross-correlation interrogation region size
Δt	interframing time
Φ	convection angle

Subscripts

j, jet	jet properties at the injection exit
x, y	Cartesian coordinates
∞	free stream

Received: 31 October 2000 / Accepted: 17 December 2001
Published online: 30 April 2002

A. Ben-Yakar (✉), R.K. Hanson
High Temperature Gasdynamics Laboratory
Stanford University
Stanford, CA 94305, USA
E-mail: adela@stanford.edu
Tel.: +1-650-7230161

Present address: A. Ben-Yakar
Stanford University, Applied Physics Department
Ginzton Lab, 450 Via Palou, S-25
Stanford, CA 94305-4085, USA

The authors gratefully acknowledge the contributions of Professor M. Godfrey Mungal to this investigation. The work has been supported by the US Army Research Office, with Dr. David Mann as the technical monitor, and the Air Force of Scientific Research, Aerospace and Materials Sciences Directorate, with Dr. Julian Tishkoff as the technical monitor.

1 Introduction

The ability to capture the time evolution of unsteady supersonic flows is critical to their understanding. Non-intrusive visualization techniques, such as schlieren and laser-based planar flow imaging, are powerful and commonly used optical methods. However, tracking the structural evolution of high-speed flows requires acquisition of images at fast (typically MHz) repetition rates. In addition, very short exposure times (20–200 ns) are required to resolve instantaneous flow features. In particular, as the spatial resolution is increased (by zooming in) to resolve the small turbulent structures, the exposure time must be further reduced to avoid the blurring of turbulent structures and the repetition rate must be increased. It is, therefore, challenging to fulfill the temporal resolution requirements of high-speed imaging while maintaining meaningful spatial resolution for supersonic flows.

Before we introduce previous and current efforts towards the development of supersonic flow visualization at ultra-fast-framing rates, it is useful to present the motivation behind such efforts. Of great interest is the study of shear layers formed at the interface of two parallel or

skewed fluid streams. Since Brown and Roshko (1974) demonstrated that large-scale coherent structures are dominant in subsonic shear layers and that their structure and evolution control the mixing process, many researchers have concentrated their efforts on measuring large-scale convection characteristics of shear layers in supersonic flows. However, most of the supersonic flow studies were limited to double-pulse visualization techniques, such as double-pulse schlieren by Papamoschou (1991), double-pulse Mie/Rayleigh scattering by Elliott et al. (1995), double-exposure planar laser-induced fluorescence (PLIF) of acetone by Papamoschou and Bunyajitradulya (1997) and Fourguette et al. (1991), and double-pulse imaging using simultaneous acetone/OH PLIF by Seitzman et al. (1994). Those studies focused on measuring the convective velocity (U_c) of large-scale structures by capturing a maximum of two images that are temporally correlated. McIntyre and Settles (1991) were the first who studied the evolution of turbulent structures in a supersonic shear layer by acquiring up to four schlieren images with different time separation ranging from 1 to 24 μs. They could measure an average convection velocity of large-scale structures within ±10% accuracy.

Of particular interest to our research is the shear layer formed when a gaseous jet interacts with a supersonic crossflow stream, an example of skewed shear layers. This is also a common fuel injection scheme in practical systems, such as a scramjet, and therefore a fundamental study of its mixing process is important. Although there have been numerous studies of the shear layer properties of two parallel streams, there have been relatively few works on jets in supersonic crossflow. Among those studies, only Gruber et al. (1997) studied the large-eddy convection characteristics of jets in supersonic crossflow, again by capturing two consecutive Rayleigh/Mie scattering images. Their results revealed the convection characteristics of helium and air jets injected into a Mach 2 crossflow. The highly compressible helium jet exhibited larger convection velocities in the near-field of the injection than the air jet of low compressibility. However, the accuracy of the velocity measurement was only about ±10%, as the minimum separation between the laser pulses was limited to 1 μs.

It is crucial to characterize the full life cycle of the jet flow-field. The near-field mixing of transverse jets is dominated by macromixing driven by jet-shear layer vortices. These large-scale eddies are formed periodically at the early stages of shear layer development and undergo structural evolution as they convect downstream. Large quantities of free-stream fluid are engulfed by the large eddies into the jet shear layer. As a result, the interface between the unmixed jet and free-stream fluids stretches. Stretching increases the interfacial area and simultaneously steepens the local concentration gradients along the entire surface while enhancing the diffusive micromixing. This might be followed by tearing mechanism of eddies when there is a large velocity gradient between the free-stream fluid and the jet (see Ben-Yakar 2000). To measure the formation frequency of these eddies and to follow their structural evolution should aid the understanding of the origin, formation and factors affecting the development of the jet vortical structure and, hopefully, provide tools in controlling its mixing properties. Such studies require application of an ultra-high-speed imaging system.

In our experiments, we therefore selected a new fast-framing imaging system capable of recording eight consecutive high-resolution schlieren images at rates up to 100 MHz. Our goal is to study the time evolution and convection properties of large-scale structures present in the shear layer of the jet/free-stream interface. It is important to understand how these structures and the shear layer growth rate vary as flow conditions and fuel types are changed. Moreover, most of the earlier jet studies were carried out in blow-down wind tunnels where the free-stream conditions were usually of low temperature and therefore had relatively low speeds. The free-stream velocity in the experiments of Gruber et al. (1997), for example, was about 515 m/s. In our experiments, we employ an impulse facility, which can generate realistic conditions of a typical supersonic combustor with high velocities (1,800–3,300 m/s) and high static temperatures (1,300 K) (A. Ben-Yakar and R.K. Hanson, 2002). However, these facilities have short test times (~0.2–2 ms), during which there is only a brief opportunity to perform a flow-diagnostic measurement. As a result, an application of MHz imaging in impulse facilities becomes almost necessary in order to obtain multiple images that are also time correlated. In our facility, the amount of data obtained per experiment is, therefore, increased by eight times by the new ultra-high-speed imaging system.

In the following sections, we present the first demonstration of the ultra-fast schlieren imaging system. Results, both qualitative and quantitative, will be summarized to demonstrate the system performance. Issues of resolution, timing, synchronization and image-processing techniques will also be discussed.

2 Previous and current high-speed imaging efforts

High-speed imaging requires two components: a camera that can acquire images at high framing rates and an intense light source with either a long time duration or a high repetition rate. Next, we shall summarize the different options of high-speed cameras and companion light sources.

The early flow visualization at high-speed framing rates was performed using a rotating mirror camera. Mahadevan and Loth (1994), for example, utilized a rotating mirror camera to temporally resolve compressible mixing layer structures at approximately 350 kHz using schlieren and Mie scattering. A xenon flash system with square pulse durations up to 200 μs was used as a continuous light source. The quality of the images was poor because of the low resolution and blurring of the images due to the convection of the flow structures.

Another possibility for high repetition-rate imaging employs the Cranz–Schardin high-speed framing technique, developed several decades ago by the German experimentalists Cranz and Schardin (1929). This

high-speed photographic system utilizes a multiple spark light source and multiobjective film camera. Essentially, an array of point sources, fired in sequence, provides both the light and shutter action required to capture images at high repetition rates up to 10 MHz (Bretthauer et al. 1990). An example of its use in supersonic turbulent mixing research was performed by McIntyre and Settles (1991). Average convective velocity of large-scale structures was measured with ±10% accuracy using ensembles of three to four consecutive schlieren images taken with interframing time separation values ranging from 1 to 24 μs.

Patrie et al. (1993,1994) performed 3-D snapshots of instantaneous flow structures using Mie scattering and laser-induced fluorescence of flames and turbulent jets. Their camera system included a high-speed image converter coupled by fiber optics to a CCD camera. Up to 20 sequential planar images were collected at the rate of 10 MHz. The output of the system was a single digital image with a 400×700-pixel format, containing the sequence of images, e.g., each image was approximately 160×140 pixels for a 10-image set. This imaging system required post-processing algorithms to correct the spatial distortion of the images caused by electrodynamic interaction of the photoelectric currents within the camera. Island et al. (1996) used the same imaging system to study the three-dimensionality of supersonic mixing layers. The planar illumination for a 3-D scan was provided from a 2-μs pulse duration, flashlamp-pumped dye laser with a pulse energy of 3 J at 590 nm. The laser output was reflected from a high-rpm rotating mirror to achieve translation of the illuminating light sheet. The pixel resolution was approximately 1 mm, so that only relatively large scales of mixing were resolved.

Recently, several researchers reported efforts toward MHz-rate digital planar flow visualization using two different MHz-rate digital cameras, one manufactured by Princeton Scientific Instruments, Inc. (PSI) and the other by Silicon Mountain Design (SMD) (now a subsidiary of Dalsa, Inc.). A prototype CCD camera manufactured by PSI with pixel format of 180×90 or 180×180 was used by several researchers including Huntley et al. (2000), Thurow et al. (2000), and Wu et al. (2000). This camera has a 32-image storage buffer built onto the image sensor chip itself and can frame at rates up to 1 MHz. The drawback of the PSI camera is the low pixel resolution of images (the pixel size is 50 μm×50 μm) and the low fill factor of the light-sensitive area, which is about 14%. PSI has attempted to develop this unique high-speed framing CCD camera under a government SBIR contract. However, further development of this prototype camera is currently not possible owing to difficulties in manufacturing the chip. The SMD MHz-rate CCD camera, currently available on the market, was recently used by Thurow et al. (2001) to investigate large-scale structures in a Mach 1.3 axisymmetric jet. The SMD camera has 240×240 pixel format and can acquire 17 images at a variable rate as fast as 1 MHz.

Both the PSI and SMD cameras are typically paired with a laser working in a pulse "burst" concept (Wu and Miles 2000). The "burst" train of 30–40 pulses was formed by applying a high-speed Pockel Cell "slicer" to the long-duration output (200 μs) from a continuous wave Nd:YAG ring laser. The energy of each of the individual pulses comprising the train was 25 mJ, with minimum separations of 1 μs (1 MHz). With this energy level of pulses, the researchers succeeded in performing CO_2-enhanced filtered Rayleigh scattering measurements in supersonic flows.

As summarized above, since the early 1990s, several research groups have attempted to perform high-speed imaging of supersonic flows. Their results showed the excellent potential of high-speed 2-D and 3-D measurements. However, their imaging systems were usually of low resolution and low light sensitivity.

In this paper, we present initial results with a new commercial imaging system that can capture images (free of distortions) at rates up to 100 MHz. The system includes a fast-framing rate camera (IMACON 468) combined with a long-duration, high-intensity light source (xenon flashlamp) to acquire eight consecutive schlieren images of supersonic flows each with a 578×384-pixel resolution. In this system, resolution and blurring of the images can be controlled by adjusting the image exposure time, which can be as short as 10 ns.

A similar fast-framing camera system with a maximum repetition rate of 1 MHz is also being used by Kaminski et al. (1999) to study turbulent reacting flames. The system performance was demonstrated at a repetition rate of 8 kHz using a custom-built unit (B.M. Industries Division, Thomas CF Laser, Totowa, N.J.) of four double-pulsed Nd:YAG lasers with an accompanying dye laser. This laser system allowed variable interframing times of 25–145 μs.

3
Experimental approach

The experiments are aimed at improving our understanding of the mixing, ignition, and flame-holding processes of fuel jets in supersonic combustion. We use an expansion tube to provide a relatively accurate simulation of the true flight conditions at the entrance of a typical supersonic combustor in the Mach 8–12 flight range (Ben-Yakar and Hanson 2002). Due to the large total enthalpies (greater than 3 MJ/kg) associated with high flight speeds beyond Mach 8, only impulse facilities are capable of providing the conditions for ground testing, typically with short test times (∼0.2–2ms). We utilize the MHz imaging system to acquire multiple images during the short test time. Although the schlieren technique has some limitations, as it integrates the effects of density gradients along the beam propagation path, it can be used to identify and track structures along the edge of the jet. Features internal to the jet can be discerned only with a planar light-sheet technique such as PLIF. Other visualization techniques used in our studies include simultaneously performed PLIF of OH radicals to map the regions of ignition and flame-holding (Ben-Yakar and Hanson 1998).

The free-stream flow conditions used in the experiments presented here replicate combustor entry conditions for Mach 10 flight and are summarized in Table 1.

Table 1. Free-stream flow conditions

Free-stream gas	M_∞	T_∞ (K)	p_∞ (kPa)	U_∞ (m/s)	γ_∞	Re_x=50 mm	δ_{bl}(mm)
Nitrogen	3.38	1,290	32.4	2,360	1.32	2.2×10^5	0.75

3.1
Expansion tube facility and injection system

An expansion tube is an impulse flow device, which can generate a wide range of high-velocity flow conditions with high total temperatures (enthalpies). The Stanford expansion tube facility with its dedicated lasers and ultra-fast-framing schlieren optical arrangement is presented in Fig. 1. The flow facility is 12 m in length, has an inner diameter of 89 mm, and includes three main sections: driver, driven, and expansion sections. The operation cycle of the expansion tube is initiated by bursting the double diaphragms, which causes a shock wave to propagate into the test gas and produce a flow of intermediate velocity with an increased pressure and temperature. The shocked test gas (in the driven section) then accelerates through the expansion section and emerges from the end of the tube. Downstream of the exit of the expansion section, a square viewing chamber of cross section 27×27 cm is mounted. This test chamber is equipped with an opposed pair of square (13×13 cm) quartz windows for observation and a fused silica window on top of the chamber for admission of the vertical laser sheet for laser-based diagnostics such as OH-PLIF.

The injection system is positioned at the exit of the expansion tube and inside the test section (Fig. 2). The system consists of a flat plate with an attached high-speed solenoid valve (less than 1 ms opening time, General Valve Series 9, Iota One controller), which allows near-constant injection flow rates during the expansion tube test time period. For the results presented here, an under-expanded transverse jet of hydrogen with a 2-mm port diameter was used. The jet port is located at a distance 30 mm downstream of the tube exit and about 50 mm downstream of the flat plate leading edge. At this location, the boundary layer thickness, developing on the flat plate, is approximately 0.75 mm for the conditions presented in this paper. Table 2 summarizes the jet flow exit properties.

3.2
High-speed schlieren imaging components

The ultra-fast-framing schlieren system illustrated in Fig. 3 comprises three components: (1) a high-speed framing camera (Imacon 468, manufactured by Hadland Photonics), (2) a long-duration light source (xenon flash-lamp), and (3) mirrors and knife edge (KE) in a standard Z-arrangement.

The IMACON 468 consists of eight independent intensified CCD cameras for high-speed framing that can capture eight consecutive images with variable exposure and interframing times down to 10 ns. The single optical

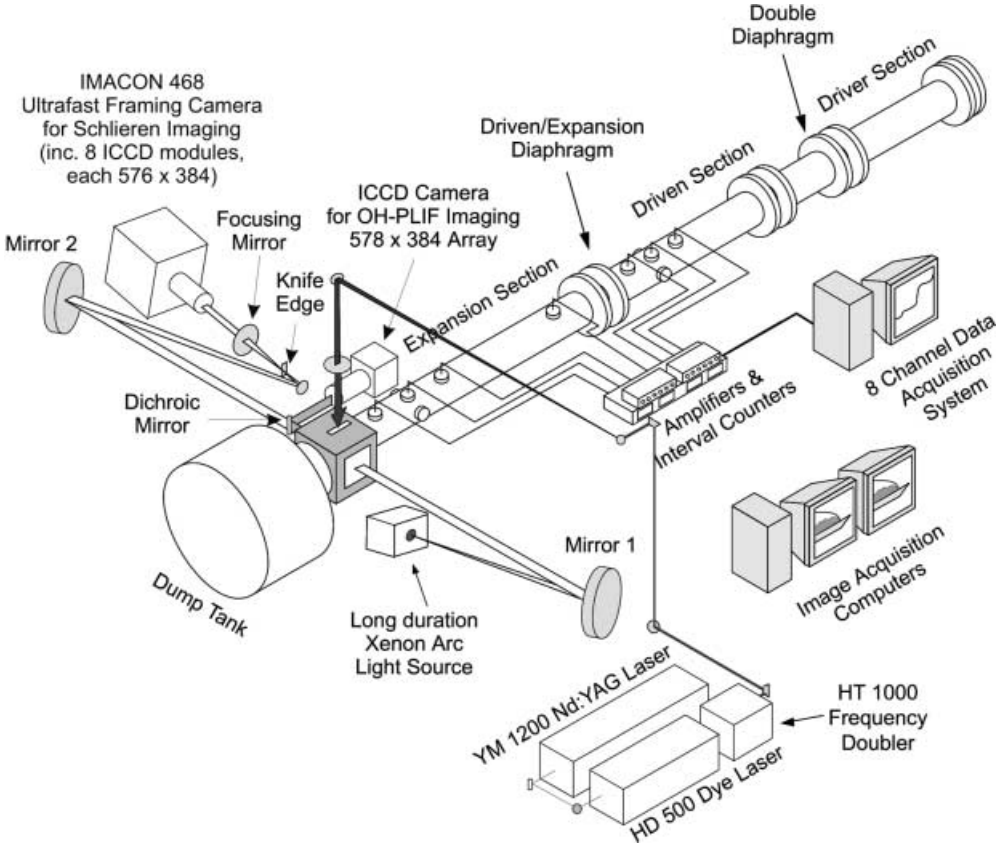

Fig. 1. Expansion tube facility (12 m in length) and imaging system

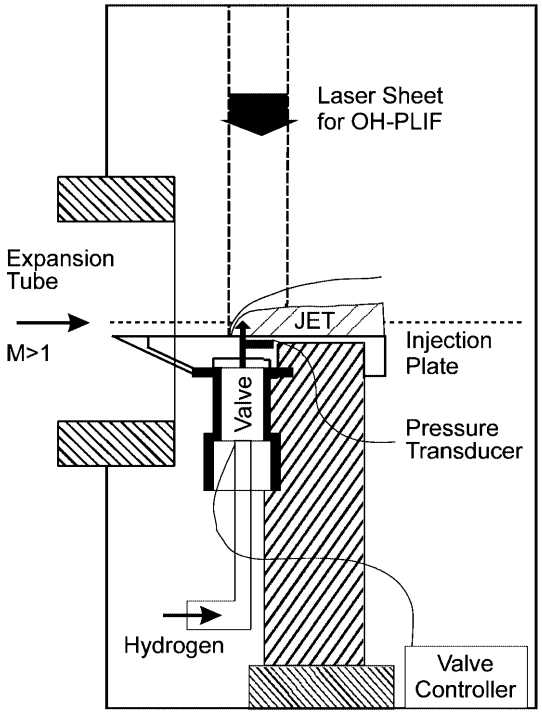

Fig. 2. Injection system schematic

input is divided uniformly by a special beam splitter and directed onto eight different intensified CCD modules, each with a 576×384 array of 22×22-μm pixels.

The light source is a high-intensity xenon flash discharge unit (Hadland Photonics model 20-50 flash system with an extension to 200-μs duration). The unit has three ranges providing 20-μs, 50-μs, and 200-μs durations, with discharge energies of 125 J, 375 J, and 700 J per pulse, respectively. This light source produces a small rectangular source image of about 2×4 mm.

In the optical set-up, two *f*/10, 200-cm focal length concave mirrors are used to collimate the light through the test section and then refocus it onto a KE (razor blade). This KE at the focal point of the second schlieren mirror is used to partially cut off the deflected rays for observing the schlieren effect (visualization of density gradients). Blocking more of the light by moving the KE transverse to the optical axis makes the system more sensitive, showing more features of the jet (Merzkirch 1965). The KE, oriented horizontally or vertically, will emphasize the density gradients in the vertical or horizontal directions, respectively. In Fig. 4, examples of schlieren images with vertical and tilted KE orientations are presented. These are the images of an underexpanded hydrogen jet issuing into quiescent air. Some differences in the details of the flow-field can be observed just by positioning the KE at different orientations. While the Mach disk is very clear in both images, the barrel shock becomes even clearer when KE is tilted (see Fig. 4b), emphasizing the horizontal density gradients as well. In our experiments, the KE is normally positioned at 45° to emphasize both the vertical and horizontal gradients.

Table 2. Jet flow conditions at the injector exit

Jet gas	M_{jet}	T_{jet} (K)	P_{jet} (MPa)	U_{jet} (m/s)	γ_{jet}	d_{jet} (mm)	Re_{djet}	J
Hydrogen	1	246	0.49	1,205	1.42	2.0	1.5×10^5	1.4 ±0 0.1

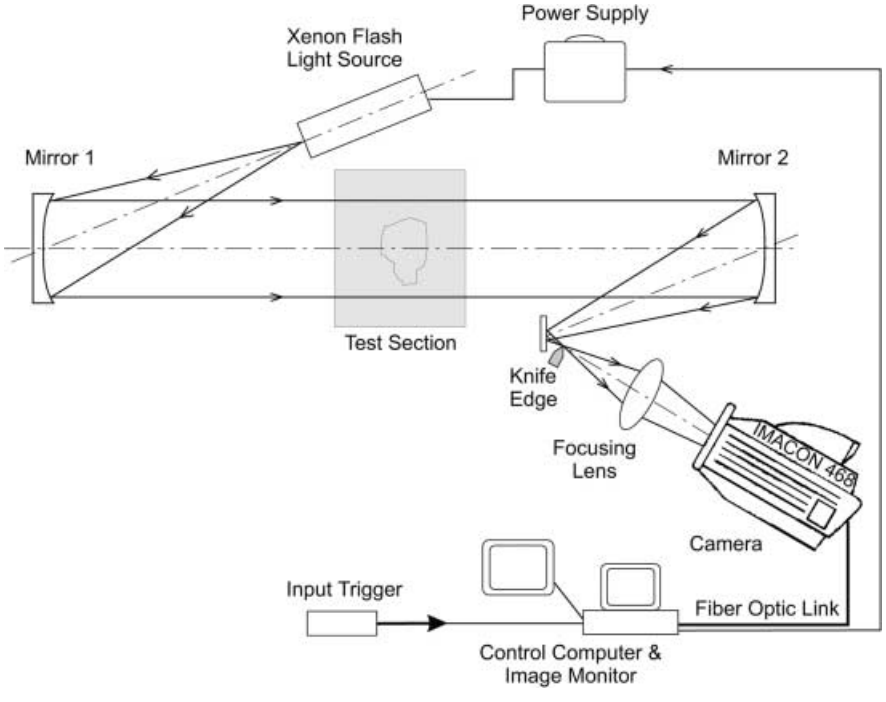

Fig. 3. Schlieren imaging set-up

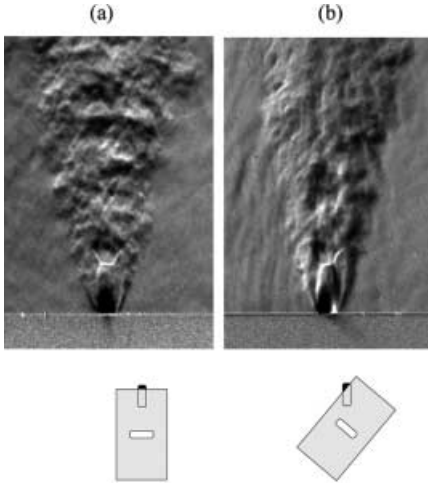

Fig. 4. **a**, **b** Examples of schlieren images of jet issuing into quiescent air as obtained for different positions of the KE (razor blade) at the focal point. We normally use the set-up demonstrated in **b**, where the KE cuts the focused light at a 45° angle to enhance both the vertical and the horizontal density gradient effects. The field of view in the images is about 50×30 mm

The test object is then imaged with a single (constant focal length) lens onto the intensified CCD cameras. Two different focal length lenses (an *f*/12.5, 100-cm focal length lens and an *f*/6, 49-cm focal length lens) were used to image different sizes of the field of interest. In this paper, a field of view of 28×18 mm was imaged onto the 12.7×8.5-mm CCD array. Therefore, a magnification of 0.44 was required and obtained using a 100-cm focal length (*f*/12.5) lens.

3.3
Timing and synchronization

Flow establishment, timing, and synchronization are important issues that have to be addressed carefully in the preparation of an experiment in an impulse facility. The imaging system must be synchronized with the facility operation, and the delay times must be set to allow the data to be acquired during the short steady test time. Therefore, test flow arrival and its steady duration are first studied through characterization experiments (Ben-Yakar and Hanson 2002) to determine the required delay times. The general approach is to replace the injection plate with a pitot probe and to trace the flow history at the injection location by analyzing pitot pressures. An example of the pitot pressure trace is given in the timing and synchronization diagram in Fig. 5. Based on the time history of this pitot pressure, it is possible to identify the arrival of the shock wave, the time period of expansion section flow, the pressure rise as the contact surface between the test gas and expansion section gas arrives, and finally the steady flow test time. The images can be acquired during the last ~100 μs of the 270-μs window of the steady flow test time, after the free-stream flow around the jet is established.

As described in Fig. 5, the imaging system and the jet flow are synchronized by the instantaneous pressure rise of one of the piezoelectric transducers located at the tube wall as the incident shock passes by. The injection system is triggered early enough to allow the injector valve to actuate and the underexpanded jet to be fully developed by the time the steady test flow conditions are obtained. The time interval between the valve actuation and the test gas arrival is short enough to avoid significant changes in the

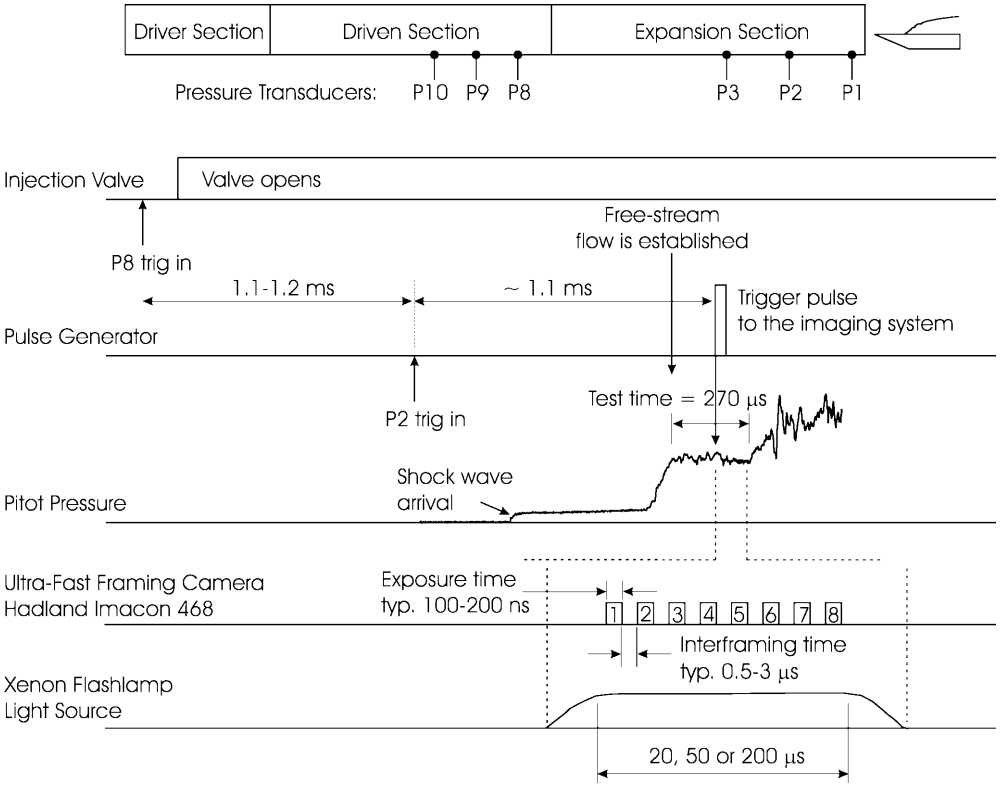

Fig. 5. Timing diagram of the high-speed imaging system and its synchronization with the expansion tube test flow time

expansion section initial pressure. The delay times for the imaging system are then set to sample during the actual test time when both the free stream (expansion tube flow) and the flow around the jet are established.

The high-speed camera, Imacon 468, and the long-duration light source receive the delayed trigger pulse simultaneously. The gating/exposure times of the eight intensifiers and their interframing times are then controlled by the image-acquisition computer. The first independent intensified charged couple device (ICCD) is set to acquire its image after the build-up time of the light source is completed and a uniform light intensity is achieved.

3.4 Resolution considerations

Each intensified CCD detector in the ultra-fast-framing camera has an 8-bit dynamic resolution (0–255 gray scale) 576×384 array with a 22×22-μm pixel size (the array dimensions are 12.7×8.5 mm). For the results presented in this paper, the field of view is normally 28×18 mm, corresponding to a minimum spatial resolution of 50×50 μm.

Visualization without blurring from the flow velocity requires careful consideration of the gating/exposure time. First the characteristic length scales and velocities of the flow-field need to be known. In our experiments, we study the time evolution of jets issuing from a 2-mm sonic orifice into a high-speed (2,360 m/s) free stream. Of particular interest are the convection characteristics of the jet-shear layer large eddies with dimensions ranging between one and two jet diameters (2–4 mm). We expect these structures to travel at speeds between that of the jet at the injector exit and the free-stream flow, namely between 1,205 and 2,360 m/s (∼1.2–2.4 μm/ns) in the case of hydrogen injection. Therefore, to achieve a 1-pixel spatial resolution (50×50 μm), the exposure time must be in the range of 42–21 ns.

The exposure time of the schlieren images in our experiments was determined by optimizing the following competing factors: (1) schlieren sensitivity, (2) spatial resolution, (3) dynamic range, and (4) signal to noise ratio. The sensitivity to detect the smallest density gradients in the flow is controlled by the KE position when the light source intensity and the optical components are fixed. As the KE cuts off more deflected rays, the schlieren sensitivity increases while less light reaches the camera. For short exposure times, a high-intensity light source is required to cover the full dynamic range (256 gray levels). Therefore, we have performed an optimization between these counteracting effects to achieve the best performance available from the system. We chose an exposure time of 100 ns to visualize a flow-field of 28×18 mm, even though shorter gating times as low as 10 ns are available in the ultra-fast-framing camera. Over a period of 100 ns, the large-scale structures can translate 120–240 μm, which is about 2–10% of their thickness (2–4 mm). This corresponds to blurring of images by 2–5 pixels. In addition, the ICCD module intensifiers were set at 30–40% of their maximum potential. We have found that larger gain results in increased noise levels that confuse the interpretation of the flow features.

Figure 6 represents three examples of schlieren images captured with different exposure times: 100 ns, 200 ns, and 3 μs. Schlieren images with a 100-ns exposure time (Fig. 6a) provide the instantaneous features of the flow field with an optimized spatial resolution (2–5 pixels). An increase in the exposure time to 200 ns (Fig. 6b) results in significant blurring of the features, as the flow structures translate larger distances (4–10 pixels). Instantaneous flow features are eventually diminished with further increase in

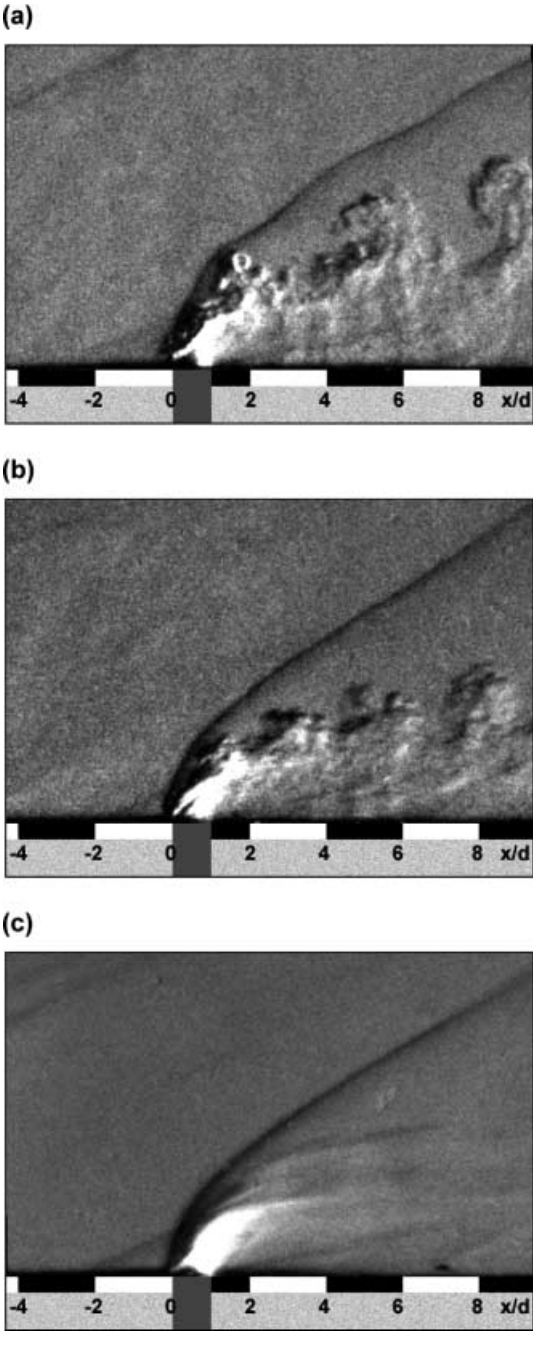

Fig. 6a–c. Examples of schlieren images with different integration/exposure times: **a** 100-ns exposure time, resolving the instantaneous features of the flow-field; **b** 200 ns exposure time, resulting in some blurring of the image; **c** 3 μs exposure time, averaging the general features while enhancing the weak shocks such as the upstream separation shock wave and downstream recompression wave

the integration time to the order of microseconds (Fig. 6c). While the instantaneous features of the flow are blurred owing to the integration of long exposure times, these images, in contrast, provide very useful information on the average features of the flow field. Note that the noise level in the long exposure image is very low, as the intensifier is set to its minimum value. Average features with pulsed-laser-based diagnostic techniques can be achieved only by capturing a large number of images, as the integration time is fixed with the laser pulse width or the fluorescence time. As noted in the introduction, it is very difficult to achieve multiple images in an impulse facility because of the short test times. Observations obtained from the schlieren images of Fig. 6 will be discussed in the following sections.

Temporal resolution, or the interframing time, was chosen so that we could capture events occurring on very short time scales, less than or equal to the convection time of the flow through the region of interest. For the jet diameter (2 mm) and free-stream velocities up to 4,000 m/s studied in our investigation, framing rates of 2 MHz to 200 kHz (interframing times between 0.5 and 5 μs) are needed to resolve and to follow the development of the flow structures (convection of large eddies, fluctuation of shock waves around the jet).

3.5
Image processing and analysis

Post-processing of the images was performed using several image-processing software packages (IPLab, Matlab, Adobe Photoshop and Premiere). Background images were acquired just prior to each test and subtracted from the schlieren image to eliminate speckle from the imperfections in the test section windows. Normalization of the intensity levels and the γ-factor were changed to improve the contrast of the images.

To compute the convection characteristics of the large-scale eddies, each individual structure was tracked with a cross-correlation method using a fast Fourier transform (FFT). In this tracking procedure, we measured the displacement of a particular feature in the streamwise and transverse directions. Guidelines for a fully automated classical cross-correlation method can be found in Smith and Dutton (1999). We utilized an FFT in our cross-correlation method to decrease the image-processing time. The velocity measurement approach taken in this paper was suggested by several researchers, such as Tokumaru and Dimotakis (1995).

The cross-correlation is calculated (see Fig. 7) from the complex conjugate multiplication of their Fourier transforms:

$$R_{fg}(\Delta x, \Delta y, \Delta t) \Leftrightarrow F(\Delta x, \Delta y, t + \Delta t)G^*(\Delta x, \Delta y, t)$$

The size of the interrogation window (128×128 pixels for the results presented in this paper) is selected manually to be large enough to include the eddy and its later location while maintaining maximum resolution. Figure 7 illustrates the cross-correlation procedure and presents a representative cross-correlation field of the two images shown in the same figure. The highest cross-correlation magnitude corresponds to the convection distance of the large-scale structure. Therefore, the correlation peak was detected by simply scanning the correlation plane R_{fg} for the maximum correlation value $R(i,j)$ and storing its integer coordinates (i,j) with an uncertainty of ±1/2 pixel. A subpixel-accurate displacement estimate could be achieved, for example, by applying three-point interpolation (Raffel et al. 1998). However, the largest

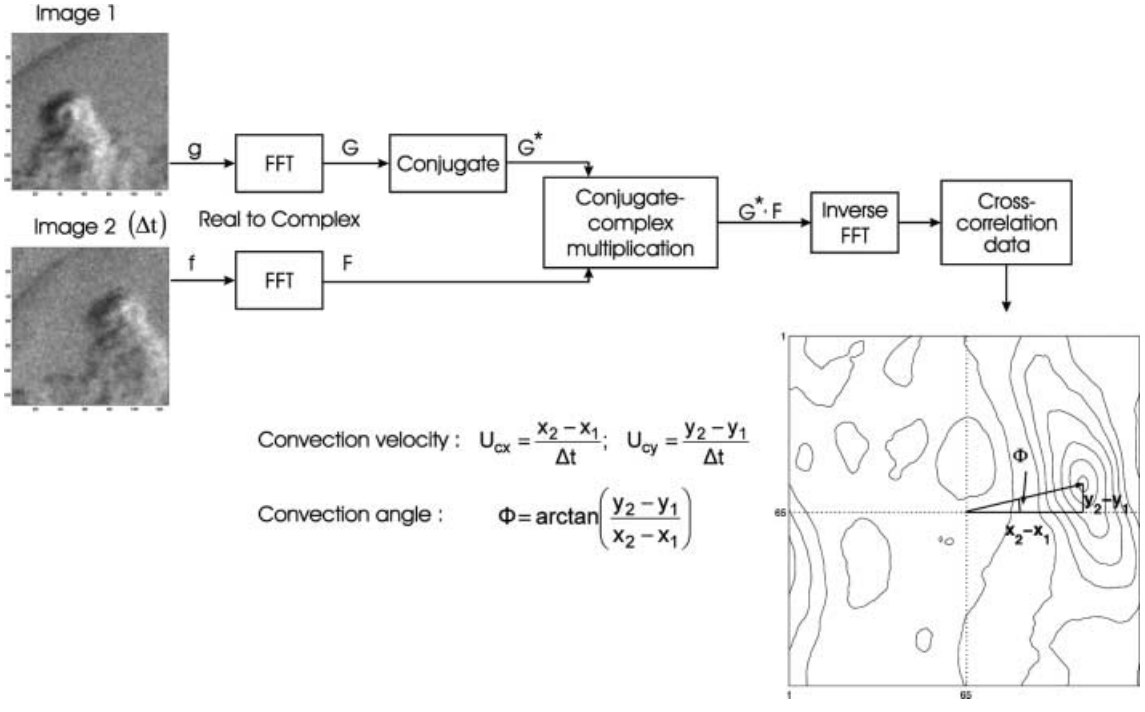

Fig. 7. Implementation of cross-correlation using FFTs to measure the convection characteristics of large eddies

uncertainty in our measurements originates in the determination of the location and the size of the interrogation region. In summary, the displacement measurement accuracy in our technique is ±1 pixel, which corresponds to a velocity uncertainty of ±50 m/s (~2% of the free-stream velocity) when the interframing time is 1 μs.

Once the displacement from image to image is known, the large-scale convection velocity and the convection angle are determined using

$$U_{c,x} = \frac{x_2 - x_1}{\Delta t},\ U_{c,y} = \frac{y_2 - y_1}{\Delta t}$$

$$\Phi = \tan^{-1}\left(\frac{y_2 - y_1}{x_2 - x_1}\right)$$

where Δt is the interframing time between images. An interframing time of Δt=1 μs was chosen based on the residence time of the eddies in the field-of-view. It takes the coherent structures about 8 μs to travel six jet diameters near the injector port (see eddy 1 in Figs. 8, 9). For

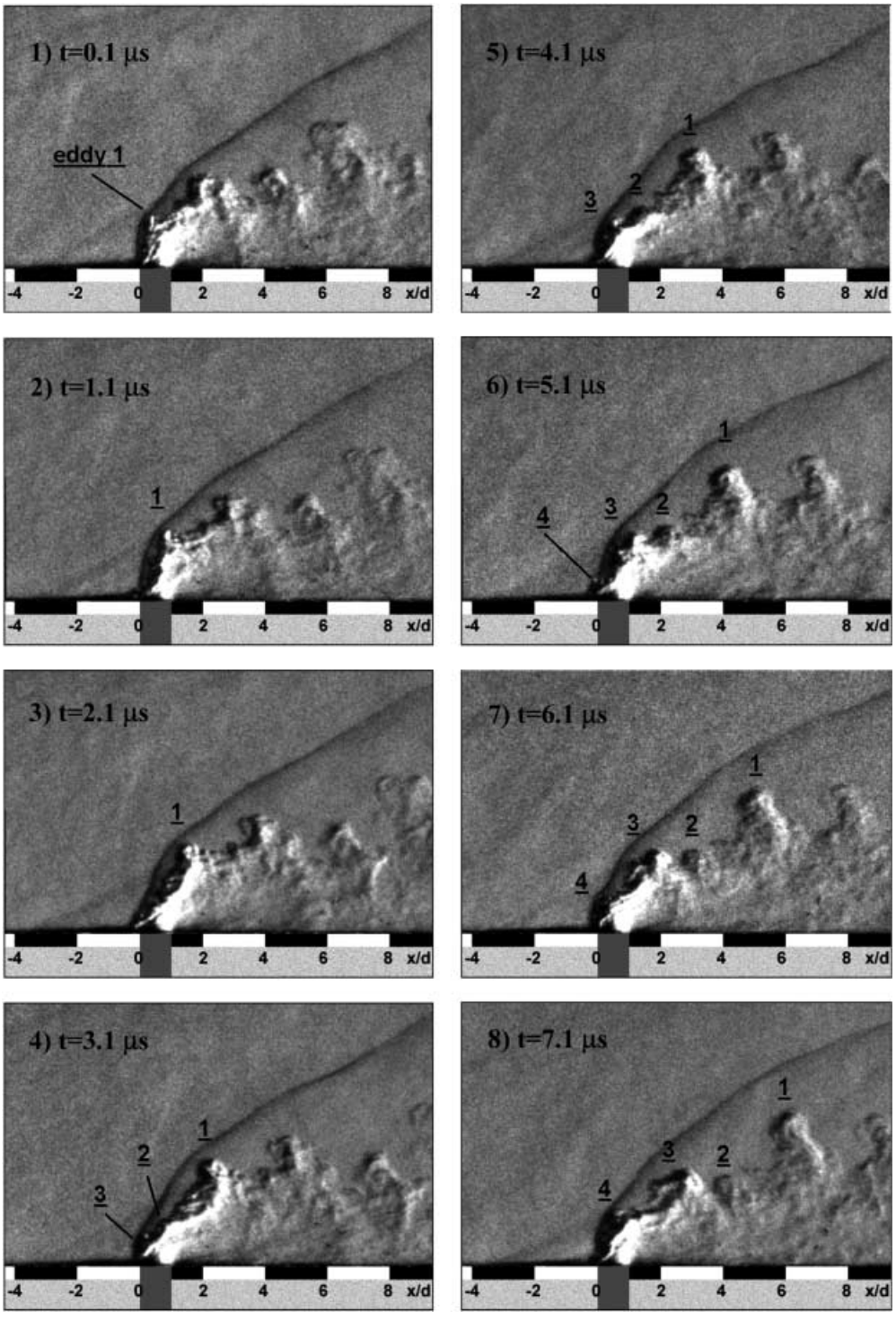

Fig. 8. An example of eight consecutive schlieren images of underexpanded hydrogen injection (d=2 mm) into a supersonic cross-flow (nitrogen) obtained by a high-speed-framing camera. Exposure time of each image is 100 ns and interframing time is 1 μs. Free-stream conditions are: U_∞=2360m/s, M_∞=3.38, T_∞=1290 K, p_∞=32.4 kPa; and jet-to-free-stream momentum ratio is: J=1.4±0.1

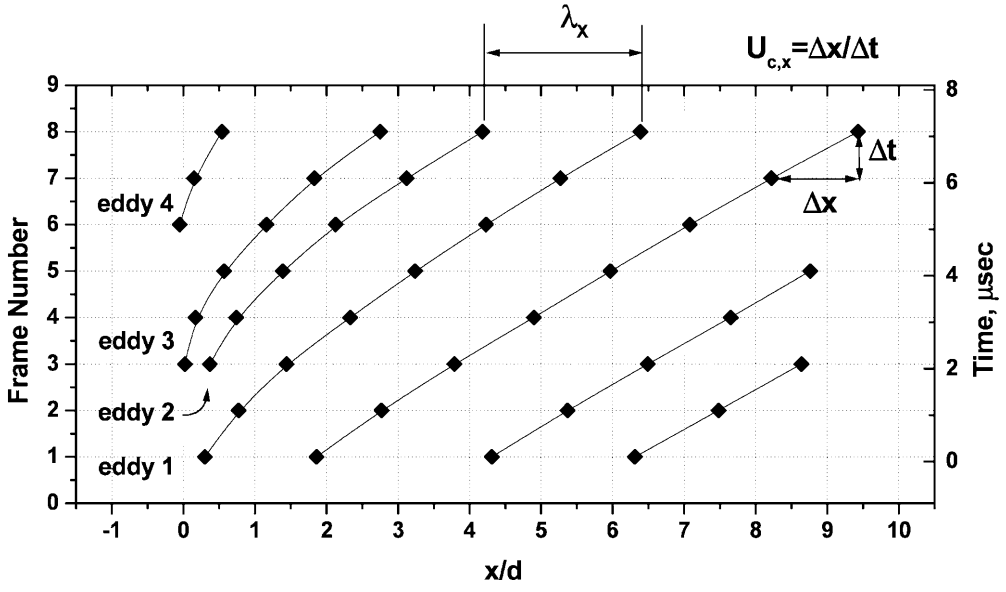

Fig. 9. The streamwise position of large-scale structures (eddies) as tracked from eight successive schlieren images (see Fig. 8), showing the time and spatial evolution of the eddies.Thus the convection characteristics of the eddies, their wavelength (the spatial gap between eddies in each frame) and the frequency of the eddy formation can be examined

interframing times greater than 3 μs, it becomes difficult to track the structures, as they travel large distances.

4
Sample data and results

Using the high-speed framing camera, we acquired schlieren images of a hydrogen jet injected into a supersonic free stream of nitrogen with a jet-to-free-stream momentum ratio of J=1.4±0.1. The free-stream and jet flow conditions in these experiments are summarized in Tables 1 and 2. An example of eight schlieren images is presented in Fig. 8. Free-stream fluid flows from left to right, and the jet fluid enters from the bottom at x/d_{eff}=0, where the effective diameter of the jet orifice is d_{eff}=2 mm. Movies of this supersonic jet interaction flow are obtained by assembling these eight consecutive images. The reader is encouraged to check the supersonic movie gallery on our web page (http://navier.stanford.edu/hanson/propulsion/scramjet/movies/t1179.html). The authors are willing to share the movies upon request.

Both qualitative and quantitative data can be obtained by analyzing these eight consecutive schlieren images. Qualitative flow-field observations reveal the structural evolution of the jet with time and how the position of shock waves in the vicinity of the jet are changed with the jet development. Among those observations, the development of the large-scale jet-shear layer vortices, similar to Brown and Roshko (1974) rollers, is one of the most important features. Mapping the positions of these eddies as a function of time into an x–t diagram provides important quantitative information in regard to the jet development. Quantitative results include the characteristics of the large-scale eddies, their convection velocity and the frequency of formation. In addition, jet penetration data and the growth rate of the jet shear layer can be deduced. Parts of this data, such as the x–t diagram and the formation frequency of the large eddies, demonstrate the unique results that can only be obtained using a high-speed-framing system.

4.1
Transverse hydrogen injection flow-field

Both short- (Fig. 8) and long-duration (Fig. 6c) schlieren images are used to study the flow-field features of the hydrogen jet injected normal into a supersonic flow. Instantaneous images with short exposure time reveal large-scale jet-shear layer vortices. These vortices are generated by the jet/free-stream interaction along the interface starting in the region near the injector exit. At this point, the injected fluid, hydrogen, moves with a higher velocity tangent to the interface than the free-stream fluid. Consequently, eddies are formed periodically. These unsteady coherent structures are less distinct when the schlieren data are integrated for a longer exposure time (3 μs), as shown in Fig. 6c.

An additional feature of the flow-field is the 3-D bow-shock around the jet, which can clearly be observed in both short- and long-duration images. While the instantaneous schlieren reveals local fluctuations in the shape of the bow-shock, long-duration schlieren demonstrates a smoother bow-shock, which also becomes slightly thicker owing to the integration of fluctuations. The frequency of these bow-shock fluctuations depends strongly on the large-scale structures of the jet. When the images are assembled into a movie, the pulsating nature of the large-scale eddies causing the bow-shock to fluctuate is very evident.

Separation shock waves upstream and downstream of the jet, which are not very clear in the short-duration images, are very apparent in the long-duration images. The separation shock wave upstream of the jet demarcates the separation of the incoming boundary layer and is important in transverse fuel injection because of its flame-holding capability in combusting situations. This low-velocity subsonic region serves as an ignition source because of the longer residence time of the crossflow which is partially mixed with the jet flow. The strength of the separation shock depends strongly on the nature of the boundary layer, that is, laminar, turbulent or transitional. The separation region for a laminar boundary layer is

much larger than the one for a turbulent boundary layer. In the present study, the jet exit is located 50 mm downstream of the flat plate leading edge. At this location, the free-stream Reynolds number is about 2.2×10^5 ($Re/m=4.3\times10^6$) and therefore is expected to be laminar. However, when we compare the eight different schlieren images from the same experiment obtained by high-speed schlieren camera, we observe some fluctuations in the size of the separation region. This observation together with the expected Reynolds number, which is very close to the critical Reynolds number, indicates that at the location of injection the coming boundary layer is likely to be transitional.

A reattachment is formed just downstream of the injection exit. As the jet expands into the free stream, it is turned further downstream to move parallel to the plate through the compression/reattachment shock.

The underexpanded jet flow, which is sonic at the orifice exit plane, initially accelerates through a Prandtl–Meyer expansion fan. The supersonic jet core is eventually compressed through a Mach disk. However, much of the flow does not pass through the Mach disk, but rather emerges from weaker oblique shocks that form the barrel shock structure around the jet. This region can be observed in the schlieren images of Fig. 4, where an underexpanded jet is issuing into quiescent air. However, the shear layer flow around the shock structures contains some unsteadiness when the underexpanded jet is injected into a supersonic crossflow owing to the periodically formed jet shear layer eddies. As a result, the structure of the barrel shock and the Mach disk are not very clear in either instantaneous or long-duration images. Only the expanding jet core-flow (the white region) is observable in the long-duration images, suggesting that the jet in our experiments is indeed underexpanded.

4.2
Time evolution and properties of large eddies

The large-scale jet shear layer vortices (the spanwise Kelvin–Helmholtz rollers) are considered important because of their role in the near-field mixing. These periodically formed eddies tend to enlarge while engulfing free-stream fluid as they travel downstream with the flow. We have observed the temporal evolution of the large eddies and measured their convection properties utilizing the high-speed schlieren camera.

The temporal evolution of large-scale structures in the streamwise direction may be visualized by an x–t diagram, which is a commonly used method to visualize wave phenomena in one dimension. Figure 9 represents the x–t diagram of large structures as tracked from the eight consecutive schlieren images shown in Fig. 8. The x axis represents the distance downstream of the jet, while the t axis represents the temporal evolution of the large eddies. The results show that four eddies are formed in 7.1 μs. Among those four eddies, eddy number 3, for example, might be formed as a result of pairing of two smaller eddies or might be a mushroom-shaped counter-rotating pair. Analysis of several experiments revealed that the formation frequency of the eddies in the hydrogen jet shear layer ranges between 513 and 663 kHz with an average value of 568 kHz. We propose that this characteristic frequency of the eddy formation is related to "the preferred mode frequency" of the jet instability (for further discussion see Ben-Yakar 2000).

After generating an x–t diagram of the eddies, the eddy parameters λ, a, b, and θ (described schematically in Fig. 10a) were measured and summarized in Fig. 10. The temporal evolution of the spacing, λ, between jet eddy cores is presented in Fig. 10b. Larger eddies rise quickly close to the jet exit, creating a spacing of almost two to three jet diameters. Occasionally, smaller eddies, such as eddy number 2, are formed. These less energetic eddies will rise more slowly and therefore their distance from the later eddy will be smaller, e.g., the spacing between eddies number 2 and 3. Owing to pairing of smaller eddies, as might have been observed during the early stages of eddy number 3 for example, λ is not necessarily a measure of the eddy formation frequency. Therefore, only high-speed framing rate imaging can provide the required information.

The dimensions (a and b) and the orientation (θ) of the eddies are plotted in Fig. 10c and d. We studied only the eddies with well-defined edges to increase the measurement accuracy, as the eddy dimensions and their orientation were measured manually. The size of large-scale structures varies between 0.5–1.5 jet diameters. The eddies become elongated (height>width) as they penetrate deeper into the crossflow, while the spatial gap between their cores increases by eddy acceleration. The gaps produced between the structures provide an important mechanism for entrainment of the free-stream fluid by the jet. As shown in Fig. 10d, the upper side of the structures is mostly tilted upstream (counterclockwise), opposite to the expected orientation. Since the crossflow velocity is higher than the jet exit velocity, it was expected that these structures would be tilted in the clockwise direction owing to the shear. However, these vortices are generated at the exit of the jet where the vertical jet velocity is higher than the free-stream velocity, therefore resulting in a counterclockwise rotation. Furthermore, the underexpanded hydrogen jet accelerates inside the barrel shock and achieves velocities that are closer to the free-stream velocity before the Mach disk. Therefore, eddies close to the jet exit entrain crossflow in-between the large-structures in the counterclockwise direction. As the jet convects further downstream, however, it is still expected that the large-scale structures will eventually exhibit a clockwise rotation due to the shear induced by the higher velocity crossflow. This phenomenon was observed clearly when ethylene gas was injected instead of hydrogen. Owing to the lower jet exit velocity associated with ethylene jets (305 m/s), the shear-induced tilting–stretching–tearing mechanism of the large structures of high-density jets (such as ethylene) is very visible (Ben-Yakar 2000).

The measured large-scale convection velocity and convection angle are presented in Fig. 11. The results indicate that large-scale Kelvin–Helmholtz rollers initially travel in the transverse direction with velocities close to the jet exit velocity (U_e=1205 m/s). From consideration of the y-momentum equation, the pressure rise behind the Mach disk implies that the jet fluid loses its momentum in the y direction. We indeed observe that the jet fluid turns to the streamwise direction be-

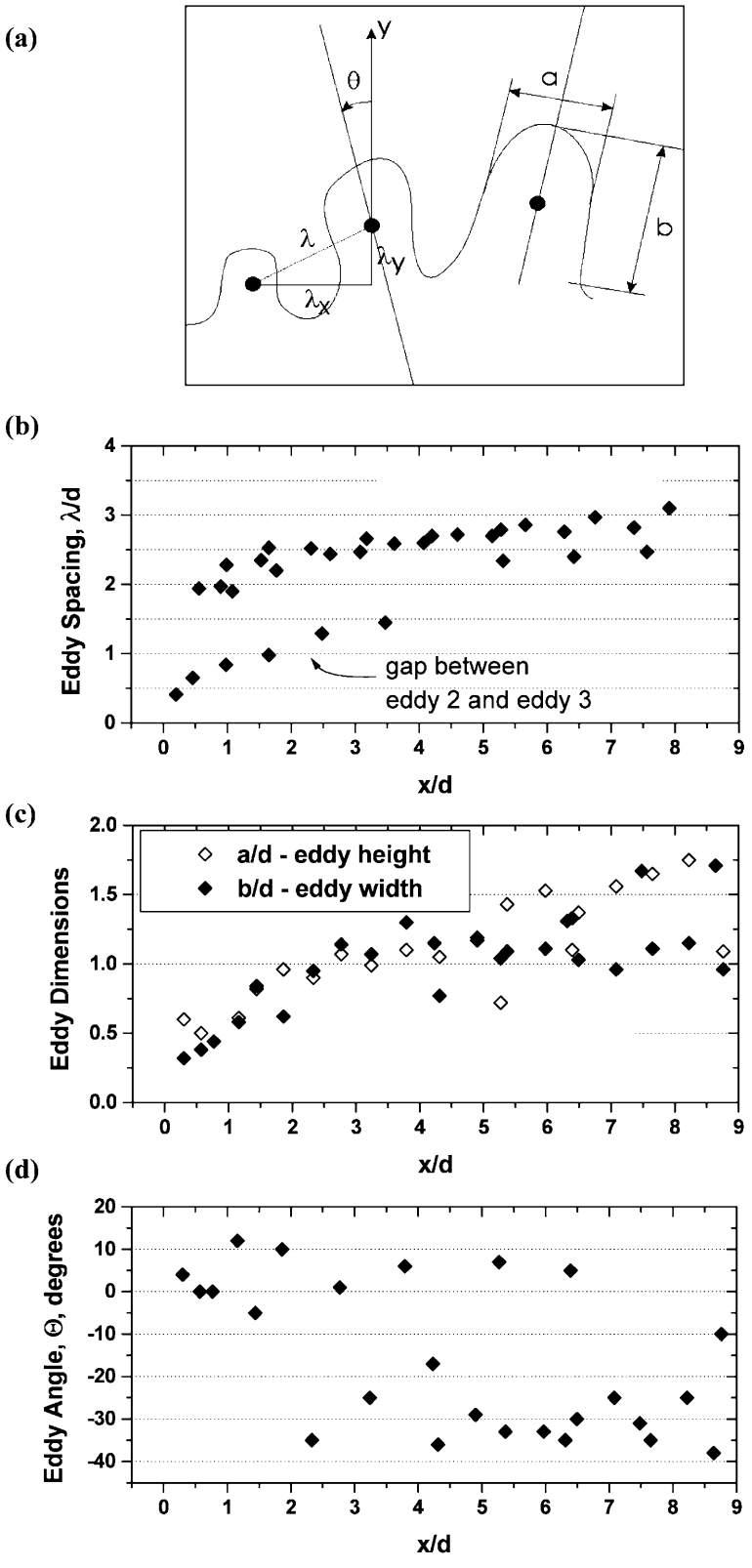

Fig. 10a–d. Eddy characteristics: **a** schematic description of eddy parameters; **b** the spatial gap between the structures (λ), termed the eddy spacing; **c** eddy dimensions (a and b); **d** the angle of the eddy orientation (θ), revealed from the analysis of eight schlieren images shown in Fig. 8

yond two jet diameters downstream right after the expected location of the Mach disk. As a result, the x component of the convection velocity starts to increase while the values of the y component decrease. These structures eventually obtain velocities ($U_c \approx 2{,}100$ m/s) near the free-stream velocity ($U_\infty = 2{,}360$ m/s) as they fully align with the free-stream flow in the far-field ($x/d > 8$). Gruber et al. (1997) studied the convection characteristics of transverse jets in a slower free-stream flow ($U_\infty = 515$ m/s). They also showed that the velocity of large eddies around helium and air jets rapidly reaches the free-stream value.

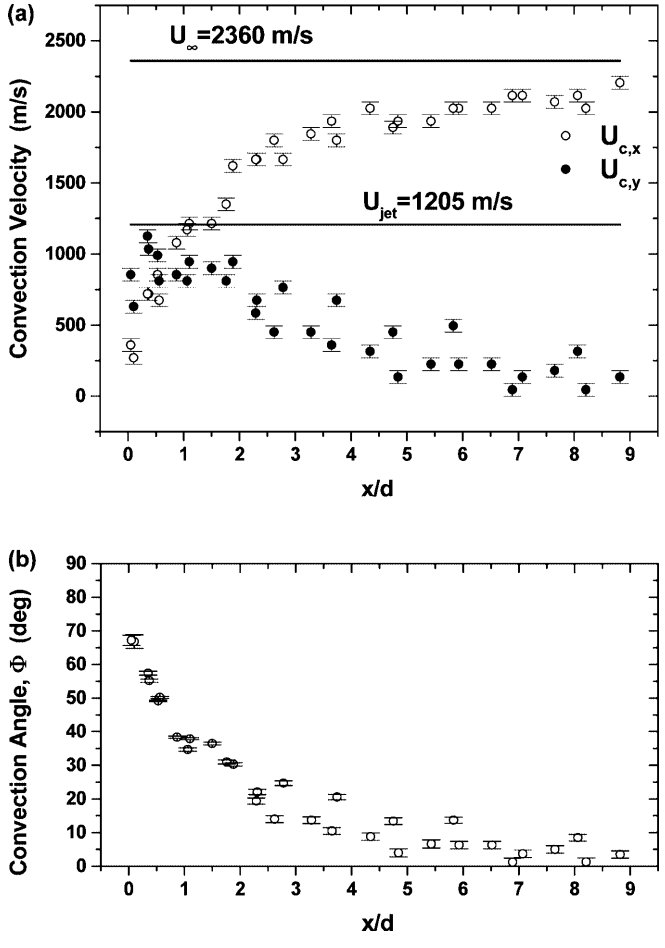

Fig. 11. Convection velocity of large-scale structures (**a**) and their convection angle (**b**), as extracted from analysis of eight consecutive schlieren images shown in Fig. 8 and traced in Fig. 9

4.3
Jet penetration and shear layer properties

As observed in the velocity measurements of Santiago and Dutton (1997), much of the jet fluid does not pass through the Mach disk, but rather emerges from the barrel shock structure forming the supersonic mixing-layer region at the top edge of the jet trajectory. The upper boundary of the jet is therefore defined by the jet-shear layer, namely by the energetic spanwise Kelvin–Helmholtz rollers which penetrate deeply into the crossflow.

We have measured the jet penetration by visual observations of the jet upper edge in the schlieren images. As plotted in Fig. 12, a penetration band is observed owing to the presence of the large-scale structures, which penetrate to a maximum height of 10–11 mm (5–5.5 jet diameters). The thickness of this band grows to about three jet diameters as the large eddies grow. At the lower region of the penetration band, we expect that pockets of pure free-stream fluid rarely exist. Therefore, we can relate the jet shear layer growth rate to the penetration bandwidth.

Jet penetration was studied by numerous authors and found to vary between studies mainly because of the variations in the approaching boundary layer properties and/or difference in the measurement techniques. Among those studies, Gruber et al. (1995) measured the jet penetration using Mie scattering of water droplets in the free stream. In their work, the outer edge of the jet was defined as 90% of the average free-stream intensity, revealing a power law fit of the form

$$\frac{y}{dJ} = 1.23\left(\frac{x}{dJ}\right)^{0.344}$$

For comparison with our measurements, plots of the above correlation are included in Fig. 12 for jet-to-free-stream momentum flux ratios of 1.4 and 2. The plots demonstrate that the Gruber's correlation for J=1.4 fell towards the lower part of the measured penetration band for the current schlieren-based data. Visual observations based on schlieren imaging mark the location of the maximum jet penetration where either pure- or mixed-jet fluid is present. Therefore, jet penetration based on schlieren imaging is expected to be somewhat larger than the jet penetration based on a conserved scalar measurement, such as Mie scattering. To determine the jet shear layer thickness, it is important to understand the near-field mixing mechanism of transverse jets. In a complementary investigation (Ben-Yakar 2000), we have shown that the jet penetration and its bandwidth (namely jet shear layer growth rate) both de-

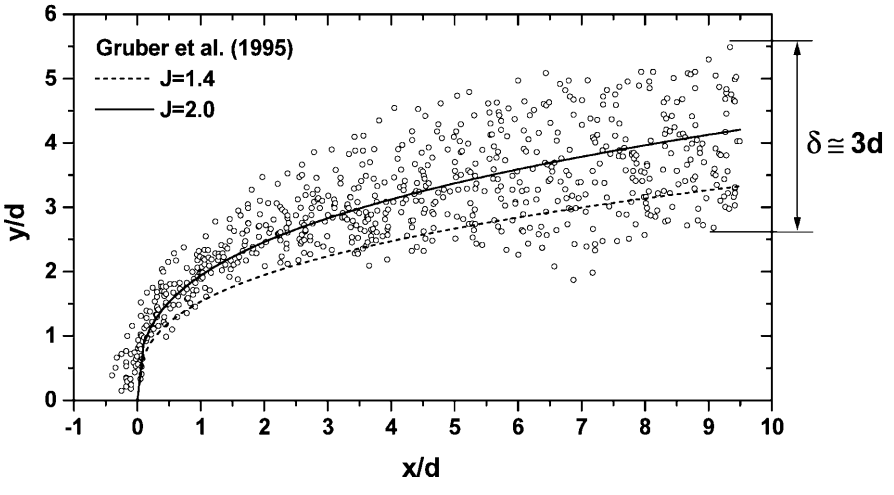

Fig. 12. Jet penetration profile obtained by measuring the outer edge of the jet (J=1.4±0.1) from eight schlieren images shown in Fig. 8. Also included in the figure are the plots of penetration suggested by Gruber et al. (1995) for comparison. The measured penetration thickness, δ=3d, is being suggested as a measure for the jet shear layer thickness

pend strongly on the jet molecular weight. A larger growth rate of the jet shear layer and therefore higher penetration was observed for jets with larger molecular weights. This was a result of the tilting–stretching–tearing mechanism induced by the large velocity gradient between the slow jet (the higher the jet molecular weight, the slower the jet exit velocity) and the fast free stream.

5
Conclusions and suggestions for future work

This paper has presented the first demonstration of an ultra-fast flow visualization system (at framing rates up to 100 MHz) based on schlieren imaging. High temporal and spatial resolutions allowed both qualitative and quantitative study of supersonic flows. The system includes a fast-framing camera (IMACON 468), capable of acquiring eight full resolution images in a 576×384-pixel format with interframing times and exposure times down to 10 ns and a xenon flashlamp system capable of providing up to a 200-μs duration of uniform light. Movies of supersonic jet injection flows were obtained by assembling the consecutive images. These movies basically slow the flow motion by one million times, allowing elucidation of the instantaneous unsteady features. For example, the pulsating nature of periodically formed eddies causing the bow-shock to fluctuate is very apparent and can easily be followed.

The performance of the system was demonstrated with a hydrogen transverse jet injected into a supersonic crossflow. For the jet diameter (2 mm) and jet and free-stream velocities (1,205–2,360 m/s) studied in this work, a framing rate of 1 MHz (interframing time of 1 μs) was used to resolve and to follow the development of the flow structures (shock waves in and around the jet and large-scale structures formed along the jet/crossflow interface). Qualitative flow observations as well as quantitative measurements such as velocity, propagation angle and formation frequency of large-eddy structures, jet penetration and the width of the jet shear layer were obtained. A cross-correlation technique using FFTs was applied to analyze the eight consecutive images.

The spatial-temporal development (x–t diagram) of unsteady structures and their frequency of formation are part of the unique database available from the analysis of time-correlated multiple images. For example, owing to pairing and stretching, the spatial gap between eddies is not necessarily a measure of the eddy formation frequency. Only high-speed imaging can provide such information, necessary for understanding the origin of the jet shear layer vortical structures which are a dominant mechanism in the near-field mixing of jets. Further investigation of transverse jets in supersonic crossflows (Ben-Yakar 2000) has revealed that the frequency of eddy formation scales linearly with the jet exit velocity, suggesting that this frequency is associated with the jet preferred mode.

We have shown that the optimization of exposure and interframing times requires consideration of four main factors, including schlieren sensitivity, spatial resolution, detector dynamic range, and signal-to-noise ratio. The imaged area was 28×18 mm and the exposure time was 100 ns. The spatial resolution was 1–2 pixel size (100×100 μm) in the near-field (x/d<2) and a maximum of 5 pixels (250×250 μm) in the far-field (x/d>8) owing to the large-scale structures movement during the exposure time. This resolving power of 2–5 pixels was achieved by optimization of the four factors discussed above. Resolution considerations become important with increasing velocities and decreasing region of interest. In our experiments, we could achieve high-quality schlieren images even though light deflections were minimum, as the jet diameter was only 2 mm. The intensified CCD cameras and the high-intensity light source provided the ability to control the sensitivity of the imaging system and achieved the required quality for quantitative data analyses.

Finally, the application of a high-framing-rate imaging system became even more important as it was combined with an impulse facility operation. The unique free-stream conditions with high speed and high temperatures studied in this investigation could only be generated for very short times. Therefore, the use of an ultra-fast schlieren system was crucial, as it significantly increased the amount of data available from a single experiment.

A broader view of our experimental efforts includes the understanding of transverse jets injected into high-speed crossflows (Ben-Yakar 2000). We observed significant differences in jet flow-field properties when the time evolution of the jet shear layer was studied in detail for different combinations of jets and free streams. The results revealed important features that were not observed in previous studies and that only became available by the application of an ultra-fast imaging system combined with the use of an impulse facility. The current ultra-fast camera, which is sensitive to visible light, can also acquire 2-D laser-based flow images such as acetone-PLIF if a high-repetition-rate UV laser light source is available.

References

Ben-Yakar A, Hanson RK (2002) Characterization of expansion tube flows for hypervelocity combustion studies. J Prop Power 18(3): in press

Ben-Yakar A (2000) Experimental investigation of mixing and ignition of transverse jets in supersonic crossflows. Ph.D. Thesis, Stanford University, Department of Mechanical Engineering

Ben-Yakar A, Hanson RK (1998) Experimental investigation of flame-holding capability of hydrogen transverse jet in supersonic crossflow. Proc Combust Inst 27:2173–2180

Bretthauer B, Meier GEA, Stasicki B (1990) An electronic Cranz–Schardin camera. Rev Scient Instrum 62:364–368

Brown GL, Roshko A (1974) On density effects and large structures in turbulent mixing layers. J Fluid Mech 64:775–816

Cranz C, Schardin H (1929) Kinematographic auf ruhendem film und mit extrem hoher bildfrequenz. Z Phys 56:147–183

Elliott GS, Samimy M, Arnette SA (1995) The characteristics and evolution of large-scale structures in compressible mixing layers. Phys Fluids 7:864–876

Fourguette DC, Mungal MG, Dibble RW (1991) Time evolution of the shear layer of a supersonic axisymmetric jet. AIAA J 29: 1123–1130

Gruber MR, Nejad AS, Chen TH, Dutton JC (1995) Mixing and penetration studies of sonic jets in a Mach 2 free-stream. J Prop Power 11:315–323

Gruber MR, Nejad AS, Chen TH, Dutton JC (1997) Large structure convection velocity measurements in compressible transverse injection flow-fields. Exp Fluids 12:397–407

Huntley MB, Wu P, Miles RB, Smits AJ (2000) MHz rate imaging of boundary layer transition on elliptic cones at Mach 8. AIAA Paper 2000-0379
Island TC, Patrie BJ, Mungal MG, Hanson RK (1996) Instantaneous three-dimensional flow visualization of a supersonic mixing layer. Exp Fluids 20:249–256
Kaminski CF, Hult J, Aldén M (1999) High repetition rate planar laser induced fluorescence of OH in a turbulent non-premixed flame. Appl Phys B 68:757–760
Mahadevan R, Loth E (1994) High-speed cinematography of compressible mixing layers. Exp Fluids 17:179–189
McIntyre SS, Settles GS (1991) Optical experiments on axisymmetric compressible turbulent mixing layers. AIAA Paper 1991-0623
Merzkirch WF (1965) Sensitivity of flow visualization methods at low-density flow conditions. AIAA J 3:794–795
Papamoschou D (1991) Structure of the compressible turbulent shear layer. AIAA J 29:680–681
Papamoschou D, Bunyajitradulya A (1997) Evolution of large eddies in compressible shear layers. Phys Fluids 9:756–765
Patrie BJ, Seitzman JM, Hanson RK (1993) Modeling of spatial distortions in a high-speed image converter camera. Rev Scient Instrum 64:2901–2904
Patrie BJ, Seitzman JM, Hanson RK (1994) Instantaneous three-dimensional flow visualization by rapid acquisition of multiple planar flow images. Opt Eng 33:975–980
Raffel M, Willert CE, Kompenhans J (1998) Particle image velocimetry. Springer, Berlin Heidelberg New York
Santiago JG, Dutton JC (1997) Velocity measurements of a jet injected into a supersonic crossflow. J Prop Power 13:264–273
Seitzman JM, Miller MF, Island TC, Hanson RK (1994) Double-pulsed imaging using simultaneous acetone/OH PLIF for studying the evolution of high-speed, reacting mixing layers. Proc Combust Inst 25:1743–1750
Smith KM, Dutton JC (1999) A procedure for turbulent structure convection velocity measurements using time-correlated images. Exp Fluids 27:244–250
Thurow B, Lempert W, Samimy M (2000) MHz rate imaging of large-scale structures within a high-speed axisymmetric jet. AIAA Paper 2000-0659
Thurow B, Hileman J, Samimy M, Lempert W (2001) An in-depth investigation of large scale structures in a Mach 1.3 axisymmetric jet. AIAA Paper 2001-0148
Tokumaru PT, Dimotakis PE, (1995) Image correlation velocimetry. Exp Fluids 19:1–15
Wu PP, Lempert WR, Miles RB (2000) MHz pulse burst laser system and visualization of shockwave/boundary layer interaction in a Mach 2.5 wind tunnel. AIAA J 38:672–679
Wu PP, Miles RB (2000) High-energy pulse-burst laser system for megahertz-rate flow visualization. Opt Lett 25:1639–1641